Title

Nanoplasmonic Phenomena at Electronic Boundaries in Graphene

Journal

ACS PHOTONICS, 4(12)

ISSN

2330-4022

Authors

Fei, Zhe
Ni, Guang-Xin
Jiang, Bor-Yuan
et al.

Publication Date

2017-12-01

DOI

10.1021/acsphotonics.7b00477

Peer reviewed

ACS Photonics

Review

pubs.acs.org/journal/apchd5

Nanoplasmonic Phenomena at Electronic Boundaries in Graphene

Zhe Fei,*[,†] Guang-Xin Ni,[‡] Bor-Yuan Jiang,[‡] Michael M. Fogler,[‡] and D. N. Basov*[,‡,§]

[†]Department of Physics and Astronomy, U.S. DOE Ames Laboratory, Iowa State University, Ames, Iowa 50011, United States

[‡]Department of Physics, University of California, San Diego, La Jolla, California 92093, United States

[§]Department of Physics, Columbia University, New York, New York 10027, United States

ABSTRACT: We review recent discoveries of the intriguing plasmonic phenomena at a variety of electronic boundaries (EBs) in graphene including a line of charges in graphene induced by a carbon nanotube gate, grain boundaries in chemical vapor deposited graphene films, an interface between graphene and moiré patterned graphene, an interface between graphene and bilayer graphene, and others. All these and other EBs cause plasmonic impedance mismatch at the two sides of the boundaries. Manifestations of this effect include plasmonic fringes that stem from plasmon reflections and interference. Quantitative analysis and modeling of these plasmonic fringes uncovered intriguing properties and underlying physics of the EBs. Potential plasmonic applications associated with these EBs are also briefly discussed.

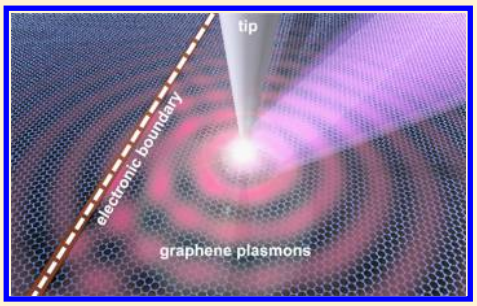

KEYWORDS: *graphene plasmons, electronic boundary, scanning plasmon interferometry, s-SNOM, plasmonic fringes*

Surface plasmon polaritons are collective oscillations of charges on the surface of metals or semiconductors.[1−4] These surface modes are in vogue for their ability to confine and control electromagnetic waves at length scales well below the diffraction limit. The search for agile plasmonic materials is a vibrant research field with promising technological applications.[5−8] Graphene emerges as a novel plasmonic medium[9−17] with many desirable characteristics including high confinement, long lifetime and broad spectral range from terahertz to near-infrared (IR).[18−46] Moreover, graphene plasmons are conveniently tunable by electrostatic gating,[18−25] photoexcitation,[36,37] magnetic field excitation,[38−40] and coupling with lattice/molecule vibrational modes.[41−46] A practical plasmonic circuit or transformation plasmonics device[47−50] demands an ability to control the flow of plasmons. Graphene offers a variety of methods for such control. Here we focus on several implementations of electronic boundaries (EBs) in graphene as well as in van der Waals coupled graphene layers and heterostructures. At these EBs, physical discontinuities are absent or play a minor role. Instead, we find evidence of nanoscale discontinuities of electronic states, which affect the propagations of electrons and plasmons across the boundaries. Even though the formation mechanisms of these EBs vary, their electronic and plasmonic responses often share some common aspects. In this review, we summarize the electronic and plasmonic responses of these EBs and discuss their fundamental physics as well as potential applications.

VISUALIZING ELECTRONIC BOUNDARIES WITH SCANNING PLASMON INTERFEROMETRY

The main method for investigating EBs discussed here is the so-called scanning plasmon interferometry,[27] implemented through a scattering-type scanning near-field optical microscope (s-SNOM). The s-SNOM is based on a tapping-mode atomic force microscope (AFM) with a metalized tip. The spatial resolution of the s-SNOM, defined by the radius of curvature of the tip apex, is typically in the order of 25 nm. As illustrated in Figure 1, the s-SNOM tip is illuminated by a p-polarized IR laser beam (blue solid arrow) and, thus, becomes strongly polarized along the direction of the tip. The polarized

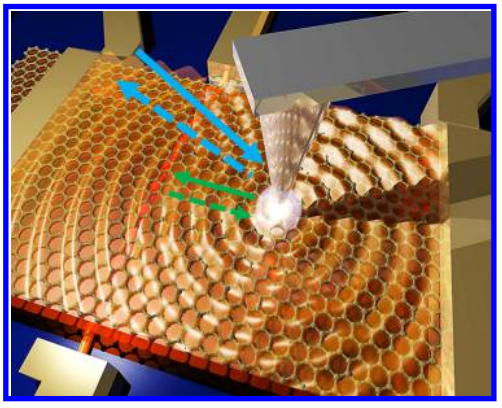

Figure 1. Illustration of the experimental study of an electronic boundary (EB) in graphene by scanning plasmon interferometry.[55] The EB is created by adding gate bias between a metallic CNT (orange line) and graphene. The blue arrows illustrate the incident and backscattered IR photons. The green arrows illustrate the tip-launched and EB-reflected graphene plasmons. Adapted with permission from ref 55. Copyright 2016 APS.

Special Issue: 2D Materials for Nanophotonics

Received: May 11, 2017
Published: June 30, 2017

DOI: 10.1021/acsphotonics.7b00477
ACS Photonics 2017, 4, 2971−2977

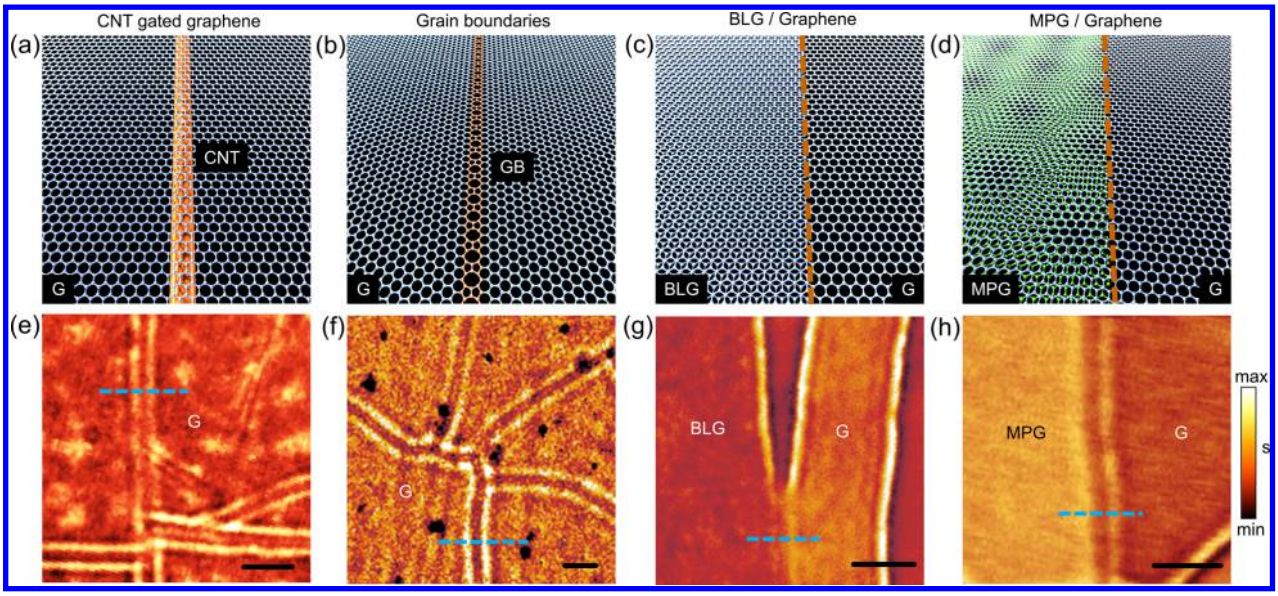

Figure 2. (a–d) Illustration of four types of EBs in graphene: charged-CNT induced EBs, grain boundaries, boundaries between BLG and graphene, and boundaries between MPG and graphene. Here "G" represents graphene and "GB" represents grain boundary. (e–h) Representative nano-IR images of the four types of EBs in (a)–(d), respectively. Here the substrate right beneath graphene is SiO_2 for (f, g) and hexagonal boron nitride for (e, h). All images were taken at ambient conditions. The excitation IR frequency is set to be about ω = 890 cm^{-1}, corresponding to a photon energy of ~110 meV. Blue dashed lines in (e–h) mark the locations where we extract the line profiles plotted in Figure 3. Scale bars in (e–h) represent 300 nm.

tip induces strong electric field underneath the sharp tip apex: the so-called "lightning rod" effect.[51] In a typical s-SNOM setup, the detector collects IR signals backscattered off the entire tip–sample system (blue dashed arrow in Figure 1). Due to the tapping of the s-SNOM tip, the intrinsic near-field signal due to the tip–sample interaction is modulated at the tapping frequency of the tip. Demodulation at the n-harmonics ($n > 1$) of the tapping frequency dramatically suppresses background signals.[52] In addition, by implementing a pseudoheterodyne interferometer,[53,54] the s-SNOM generates both the amplitude and phase components of the near-field signal. Here we focus on the third-harmonic demodulated near-field amplitude (s) to discuss the EBs.

In addition to the strong field enhancement, the sharp s-SNOM tip also enables coupling to a wide range of in-plane momenta q,[19] so it becomes feasible to launch surface plasmon polaritons in graphene. These plasmonic waves propagate radially away from the tip and reflect back when they encounter abrupt changes of sample geometry, such as physical edges or sizable defects.[23,24] Alternatively, plasmon reflection and refraction could also occur at the EBs (Figure 1) due to the impedance mismatch of plasmons caused by the disparities of plasmon wavelength (λ_p) or damping rate (γ_p) at the boundaries. Consequently, there exists two major paths for collecting backscattered photon signals. In path 1, the IR photons are scattered back directly by the tip. In path 2, part of the incident photons transfer into plasmons, propagate toward (green solid arrow in Figure 1) the reflectors, reflect back (green dashed arrow in Figure 1), and then get scattered into IR photons by the tip. Photon signals collected by the detector from paths 1 and 2 have a phase delay that scales with the distance between the tip and the plasmonic reflector. Therefore, as the tip scans toward the reflectors, one expects interference fringes parallel to the line-shaped reflectors in raster-scanned near-field images.[23,24] The period of the fringes is half the plasmon wavelength. By analyzing quantitatively the patterns of these fringes, it is feasible to extract the electronic/plasmonic properties of graphene and the EBs.

Figure 2 displays four types of boundaries and the corresponding scanning plasmon interferometry images visualizing these boundaries. The first type of boundaries are induced by electrically charged carbon nanotubes (CNT) (Figure 2a).[55] In these devices, graphene and metallic CNTs (diameter ≈ 1 nm) are separated by an ultrathin hexagonal boron nitride (hBN) layer (thickness ≈ 10 nm). Electronic discontinuities were created and tuned by gate bias between graphene and CNTs. Note that this type of boundaries are purely electronic since there are no topographic or crystalline discontinuities in graphene. The second type are graphene grain boundaries[56] (Figure 2b), which are atomic-scale line defects that connect adjacent single-crystal domains in large-area samples typically grown by the chemical vapor deposition (CVD) methods.[57] Depending on the relative mis-orientation angle between the two adjacent domains, grain boundaries could have different atomic structures. As an example, in Figure 2b we illustrate a "5–5–8" grain boundary with zero mis-orientation angle. The third type are the boundaries between graphene and bilayer graphene (BLG; Figure 2c).[58,59] Similar to graphene, BLG also supports IR plasmons but with different wavelengths, damping rates, and gating responses. Moreover, the stacking order of the two graphene layers in BLG can radically modify their plasmonic responses.[59] The impedance mismatch between plasmons in BLG and graphene is responsible for the observed plasmon refraction[58] and reflection[59] of the BLG/graphene boundaries. The fourth type of boundaries are between graphene and moiré-patterned graphene (MPG) on a hexagonal boron nitride (hBN) substrate (Figure 2d).[60] The moiré superlattices appearing in the graphene/hBN heterostructures provide periodic modulations of Dirac quasiparticles. As a result, a number of Dirac mini-bands emerge in the electronic structure leading to a variety of interesting optical and electronic effects.[61–66] The plasmonic responses of MPG

DOI: 10.1021/acsphotonics.7b00477
ACS Photonics 2017, 4, 2971–2977

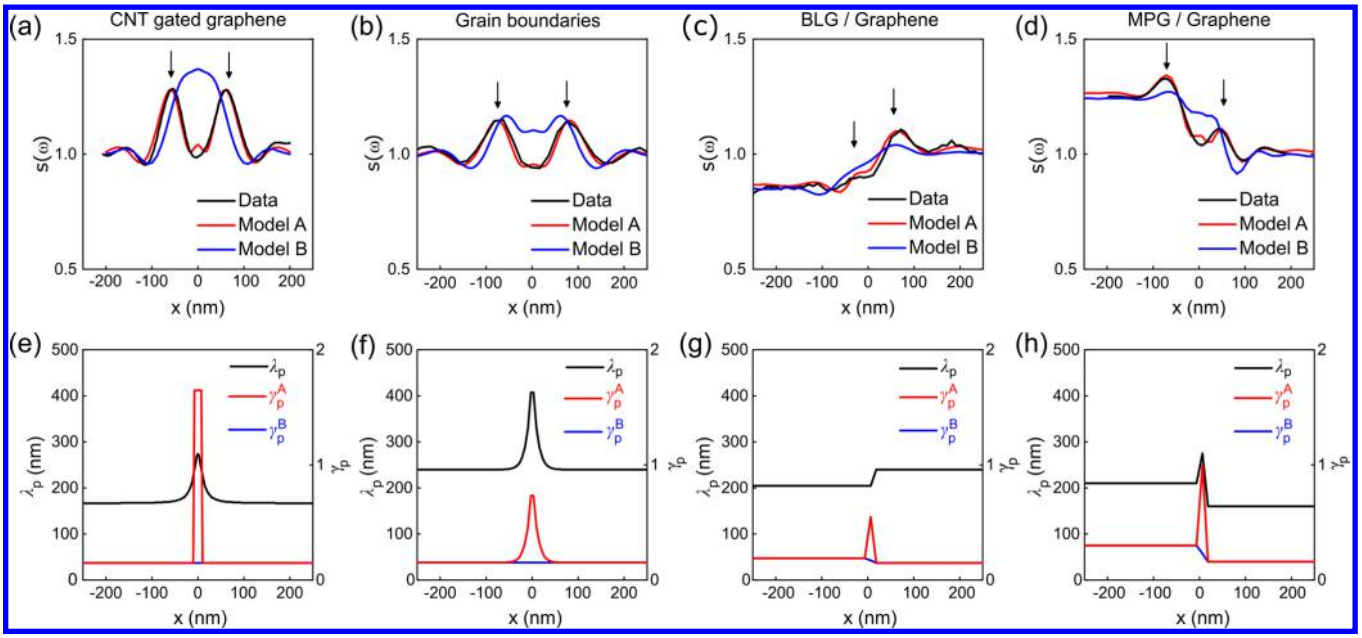

Figure 3. (a–d) Experimental (black curves) and modeling profiles (A and B) of near-field amplitude s across the parallel fringes due to the four types of EBs. The experimental profiles were extracted directly from data images in Figure 2e–h along the blue dashed lines. The peaks (marked with arrows) in the profiles correspond to the principal fringes in Figure 2. (e–h) The parameters of plasmon wavelength (λ_p) and damping rate (γ_p) used to calculate the fringe profiles. Modeling A and B share the same λ_p but different γ_p. There are additional sharp peak features at $x = 0$ in the γ_p profiles for modeling A (γ_p^A) compared to B (γ_p^B).

are also strongly modified by these superlattice mini-bands. Therefore, plasmonic impedance mismatch exists for the graphene/MPG boundaries. Compared to the EBs induced by charged CNTs, the other three types of boundaries do have structural features, but the sizes of these features are in the atomic length scale, orders of magnitude smaller than the typical plasmon wavelength of graphene in the mid-IR regime ($\lambda_p \sim 200$ nm). Therefore, their plasmonic responses, as discussed in detail below, are predominantly due to the electronic properties of these boundaries.

Representative near-field images visualizing the four types of EBs are displayed in Figure 2e–h, where we plot the near-field scattering amplitude $s(\omega)$ taken at the IR frequency of $\omega \approx 890$ cm^{-1}, corresponding to a photon energy of ~110 meV. Pairs of parallel fringes are evident in all four nano-IR images. According to previous studies,[27,29,67] these fringes are generated due to plasmon reflections off nanoscale boundaries located between the two fringes. Compared to the graphene edges, the grain boundaries and other EBs discussed here are much weaker plasmonic reflectors. Therefore, in most cases, only the first dominant plasmonic fringe is apparent on each side of the boundary. From the parallel fringes patterns in Figure 2e, one can tell that there are multiple charged CNTs underneath graphene. The distribution of grain boundaries can also be visualized in Figure 2f, where the average grain size defined by the grain boundaries is a few microns.

In the case of BLG/graphene (Figure 2g) and also MPG/graphene (Figure 2h) boundaries, clear contrast in the near-field amplitude s on the two sides of the boundaries appears. For BLG, the overall s signal is weaker than graphene.[59] Note that weaker s is typical for AB-stacking (or Bernal-stacking) BLG. For randomly stacked BLG with no or weak interlayer coupling, s is higher than graphene.[58,59] The s signal of MPG, on the other hand, is higher than graphene at $\omega = 890$ cm^{-1} (Figure 2h). Nevertheless, the contrast between MPG and graphene is frequency dependent. At $\omega = 1550$ cm^{-1}, one cannot clearly distinguish MPG from graphene.[60] As discussed in previous works,[59,60] the overall s signal is closely linked to the optical/plasmonic parameters of the interior of samples. In order to determine the properties of individual EBs, quantitative analysis and modeling of the complete patterns of the parallel plasmonic fringes are needed.

QUANTIFYING PLASMONIC PARAMETERS AT ELECTRONIC BOUNDARIES

The details of the parallel fringes associated with the four types of EBs can be viewed more clearly in Figure 3a–d, where line profiles (black curves) taken perpendicular to the fringes (along blue dashed lines in Figure 2e–h) are plotted. These line profiles were obtained by averaging over tens of separate scans across the EBs to minimize noise. The bright parallel fringes in the nano-IR images (Figure 2e–h) appear as two principal peaks (marked with the arrows) in Figure 3a–d aside the EBs centered at $x = 0$. There are also possibly weaker subsequent peaks further away from the EBs in the interior of the domains. From Figure 3a,b, one can see that plasmonic fringes at both CNT-induced EBs and grain boundaries have symmetric profiles with respect to the EBs. The two principal peaks have roughly equal intensities and widths, so they are referred to as twin fringes.[27,55] On the contrary, the fringe profiles of the BLG/graphene and MPG/graphene boundaries are asymmetric (Figure 3c,d). As discussed below, the asymmetric profiles are mainly due to the different plasmon wavelengths and damping rates at the two sides of the boundaries.

In order to model the experimental fringe profiles, we approximated the AFM tip as a highly elongated metallic spheroid (Figure 4).[23,27,37,55,68,69] The radius of curvature at the tip apex (a) is about 25 nm according to the tip manufacturer. The length of the spheroid ($2L$) is set to be 500 nm, which is not a very sensitive parameter in the modeling so long as $2L \gg$

DOI: 10.1021/acsphotonics.7b00477
ACS Photonics 2017, 4, 2971–2977

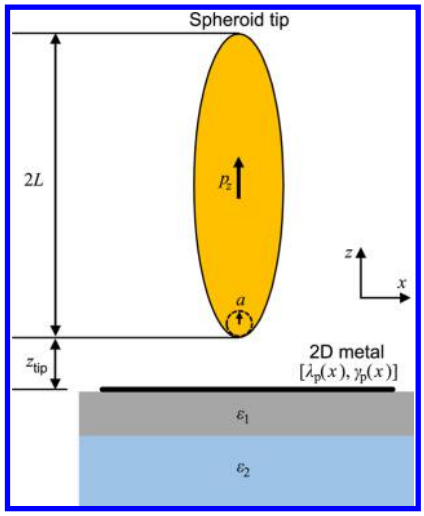

Figure 4. Sketch of the spheroid model that we used to model the nano-IR plasmonic responses of the electronic boundaries in graphene.

a. The near-field signal was calculated by evaluating numerically the z-component of the total radiating dipole of the spheroid (p_z). For simplicity, we did not consider the x-component of the dipole moment (p_x) in our calculation, which is a reasonable approximation considering $p_x \ll p_z$ in the case of highly elongated tip ($2L \gg a$). In order to obtain the third harmonic near-field signals, we considered the tip modulation and demodulation processes by computing p_z at multiple tip−sample separations (z_{tip}). The real-space profiles of third harmonic amplitude $s(x)$ were obtained by varying the x locations of the tip in the calculations.

The sample was treated as a two-dimensional (2D) metal (Figure 4) and the modeling parameters of the sample and the EBs are the x-dependent plasmon wavelength [$\lambda_p(x)$] and damping rate [$\gamma_p(x)$; Figure 3e−h]. We assume uniform sample properties along the y direction. According to previous studies,[23,27,55] λ_p and γ_p are directly linked to the real (σ_1) and imaginary (σ_2) parts of optical conductivity of graphene or other 2D metals: $\lambda_p \approx (4\pi^2/\omega\kappa)\sigma_2$; $\gamma_p \approx \sigma_1/\sigma_2 + \kappa_2/\kappa_1$. Here κ_1 and κ_2 are the real and imaginary parts of the complex effective dielectric function (κ) of the sample environment. For simple device structure, where the sample is sandwiched by air and thick SiO_2 layer, κ equals to the average of permittivity of air and SiO_2. For complicated device structures, κ has to be evaluated numerically. Within the Drude approximation, λ_p is roughly proportional to the Fermi energy (E_F) of graphene or graphene layers. The plasmon damping rate γ_p could be due to charge scatterings, interband transitions, or bound electron states (see discussions below). Therefore, the optical/electronic properties of the EBs can be directly read out from the two plasmonic parameters.

In Figure 3a−d, we plot two sets of modeling profiles (labeled as A and B) together with the experimental profiles (black curves). The A profiles (red curves) are our best fits for the data. The B profiles (blue curves) illustrate the effect of changing some of the adjustable parameters in the fits: a procedure that helps to decipher the physical origin of the observed fringe patterns as we will detail below. From Figure 3e−h, one can see that modeling A (red) and modeling B (blue) share the same λ_p parameters. Their differences are due to the unequal γ_p parameters close to the EBs ($x = 0$). Away from the boundaries ($|x| \gg 0$), λ_p of graphene is close to 200 nm, a typical value for highly doped samples at ambient conditions. The λ_p of Bernal-stacking BLG (Figure 3g) is slightly smaller than that of monolayer graphene: a consequence of interlayer electron tunneling.[59] Moiré-patterned graphene has a slightly larger λ_p but a much higher γ_p compared to graphene in the same specimen. Such a high damping originates from interband transitions associated with the moiré superlattice mini-bands.[60] The extracted plasmonic parameters close to the EBs ($x \approx 0$) are more complicated. For example, λ_p peaks appear at EBs ($x = 0$) for CNT-gated graphene, grain boundaries, and also MPG/graphene samples indicating charge accumulations at these EBs. Additional doping is expected for CNT-induced EBs due to the electrostatic gating. As for grain boundaries and MPG/graphene boundaries, the doping might be related to impurities or defects at both boundaries. The γ_p profiles of modeling A that produces the best fits of the data also show peak features at all four types of EBs. As a comparison, modeling B without γ_p peaks at $x = 0$ cannot fit well the experimental profiles. The origin of the enhanced γ_p at the charged-CNT induced EBs is attributed to the electron states bound to the 1D potential well created by the CNT.[55] Physical mechanisms behind the sharp damping peaks of other three types of EBs are not fully understood yet. Possible origins include high densities of defects and impurities close to the boundaries as well as electron bound states.

CONCLUSIONS AND OUTLOOK

The nanoplasmonic studies discussed here provide us opportunities to investigate the intriguing physics of EBs. For example, the CNT-induced EBs are model systems for exploring in a controlled way the properties of 1D bound electron states. In addition, at higher frequencies, one would expect to see hybridization effects between Dirac plasmons in graphene and Luttinger-liquid plasmons in CNT.[70] Grain boundaries harbor rich physics related to their electronic/plasmonic properties. Depending on their atomic structures, grain boundaries could support valley-polarized charge transport,[71] correlated magnetic states,[72] low-energy van Hove singularities that are signatures of 1D localized states,[73] and 1D charge ordering.[74] Future nano-IR studies of grain boundaries at cryogenic and vacuum conditions could possibly uncover these interesting physics. Recently, the photocurrent nanoscopy, which is developed by combing s-SNOM with electrical read-out, was used to study graphene grain boundaries and their impact on charge inhomogeneities and local thermoelectric properties.[75] The same technique has also been adopted to image graphene plasmons and map their dispersion relation in the terahertz frequency region.[35]

The EBs discussed above are only a representative subset of potentially a much larger group. There are indeed many other types of EBs that show intriguing electronic and plasmonic responses. For example, soliton domain walls between AB- and BA-stacked BLG were proven to be EBs that support protected chiral edge states of quantum valley Hall insulators.[76] Plasmonic fringes have also been observed close to these soliton domain walls and the fringe patterns are clearly different at the tensile- and shear-type of solitons.[77] Future studies are needed to explore the electronic origin of the unique plasmonic responses of these soliton domain walls. Another type of EBs are the junctions created by split gates above or below graphene.[35,78−80] These split gates allow independent control of graphene carrier densities on the two sides of the junctions.

DOI: 10.1021/acsphotonics.7b00477
ACS Photonics 2017, 4, 2971−2977

Therefore, one could conveniently achieve graphene p−n junctions by using split-gate device geometry. Graphene p−n junctions have attracted a lot of research interests due to their unique electronic properties including precise electron focusing and Klein tunneling.[78−80] They are also promising for applications related to graphene plasmons[35] and transformation optics.[47]

The plasmonic phenomena at the EBs in graphene promise a number of applications. For instance, tunable plasmon reflection of EBs induced by charged CNTs[55] offers the possibility of realizing the smallest possible plasmonic transistor with a channel length (boundary width) of a few nanometers. The MPG/graphene boundaries,[60] which is a typical example of plasmonic reflectors produced by layer stacking, are potential "plasmonic filters": low-energy plasmons will be reflected whereas high-energy plasmons will propagate freely through the boundaries. Moreover, the plasmonic reflectivity of the MPG/graphene boundaries are conveniently tunable by a single continuous back gate. The BLG/graphene boundaries, due to the observed plasmon refraction and reflection effects,[58,59] could be used as two-dimensional "optical" elements enabling manipulation of the propagation direction of graphene plasmons on a chip. We conclude that control of plasmonic reflections and plasmonic flow discussed here is not unique to graphene. Similar effects are likely to be observed in other two-dimensional materials including transition-metal dichalcogenides and black phosphorus. Intriguing electronic boundary effects in plasmonic transport are also anticipated in anisotropic 2D materials.[81]

AUTHOR INFORMATION

Corresponding Authors

*E-mail: zfei@iastate.edu.
*E-mail: db3056@columbia.edu.

ORCID

Zhe Fei: 0000-0002-7940-5566

Notes

The authors declare no competing financial interest.

ACKNOWLEDGMENTS

Research on static plasmon interferometry of high-mobility graphene is supported by DOE-BES DE-FG02-00ER45799. Work on plasmonic circuits is funded by ONR N00014-15-1-2671 and AFOSR FA9550-15-1-0478. The development of nanoimaging is supported by ARO−DURIP. D.N.B is supported by the Gordon and Betty Moore Foundation's EPiQS Initiative through Grant GBMF4533. Z.F. acknowledges support from Iowa State University and Ames Laboratory that is operated for the U.S. DOE by Iowa State University under Contract # DE-AC02-07CH11358.

REFERENCES

(1) Atwater, H. A. The Promise of Plasmonics. *Sci. Am.* **2007**, *296*, 56−62.
(2) Stockman, M. I. Nanoplasmonics: the Physics Behind the Applications. *Phys. Today* **2011**, *64*, 39−44.
(3) Maier, S. A. *Plasmonics: Fundamentals and Applications*; Springer, 2007; Ch. 4.
(4) Schuller, J. A.; Barnard, E. S.; Cai, W.; Jun, Y. C.; White, J. S.; Brongersma, M. L. Plasmonics for Extreme Light Concentration and Manipulation. *Nat. Mater.* **2010**, *9*, 193−204.
(5) Tao, A.; Sinsermsuksakul, P.; Yang, P. Tunable Plasmonic Lattices of Silver Nanocrystals. *Nat. Nanotechnol.* **2007**, *2*, 435−440.
(6) Boltasseva, A.; Atwater, H. A. Low-loss Plasmonic metamaterials. *Science* **2011**, *331*, 290−291.
(7) Naik, G. V.; Shalaev, V. M.; Boltasseva, A. Alternative Plasmonic Materials: Beyond Gold and Silver. *Adv. Mater.* **2013**, *25*, 3264−3294.
(8) Comin, A.; Manna, L. New Materials for Tunable Plasmonic Colloidal Nanocrystals. *Chem. Soc. Rev.* **2014**, *43*, 3957−3975.
(9) Ryzhii, V.; Satou, A.; Otsuji, T. Plasma Waves in Two-Dimensional Electron-Hole System in Gated Graphene Heterostructures. *J. Appl. Phys.* **2007**, *101*, 024509.
(10) Jablan, M.; Buljan, H.; Soljačić, M. Plasmonics in Graphene at Infrared Frequencies. *Phys. Rev. B: Condens. Matter Mater. Phys.* **2009**, *80*, 245435.
(11) Koppens, F. H. L.; Chang, D. E.; Javier García de Abajo, F. Graphene Plasmonics: A Platform for Strong Light-Matter Interactions. *Nano Lett.* **2011**, *11*, 3370−3377.
(12) Grigorenko, A. N.; Polini, M.; Novoselov, K. S. Graphene Plasmonics. *Nat. Photonics* **2012**, *6*, 749.
(13) Bao, Q.; Loh, K. P. Graphene Photonics, Plasmonics, and Broadband Optoelectronic Devices. *ACS Nano* **2012**, *6*, 3677−3694.
(14) Basov, D. N.; Fogler, M. M.; Lanzara, A.; Wang, F.; Zhang, Y. Colloquium: Graphene Spectroscopy. *Rev. Mod. Phys.* **2014**, *86*, 959−994.
(15) Low, T.; Avouris, P. Graphene Plasmonics for Terahertz to Mid-Infrared Applications. *ACS Nano* **2014**, *8*, 1086.
(16) Basov, D. N.; Fogler, M. M.; García de Abajo, F. J. Polaritons in van der Waals Materials. *Science* **2016**, *354*, 195−195.
(17) Low, T.; Chaves, A.; Caldwell, J. D.; Kumar, A.; Fang, N. X.; Avouris, P.; Heinz, T. F.; Guinea, F.; Martin-Moreno, L.; Koppens, F. Polaritons in Layered Two-Dimensional Materials. *Nat. Mater.* **2017**, *16*, 182−194.
(18) Ju, L.; Geng, B.; Horng, J.; Girit, C.; Martin, M.; Hao, Z.; Bechtel, H. A.; Liang, X.; Zettl, A.; Shen, Y. R.; Wang, F. Graphene Plasmonics for Tunable Terahertz Metamaterials. *Nat. Nanotechnol.* **2011**, *6*, 630−634.
(19) Fei, Z.; Andreev, G. O.; Bao, W.; Zhang, L. M.; McLeod, A. S.; Wang, C.; Stewart, M. K.; Zhao, Z.; Dominguez, G.; Thiemens, M.; Fogler, M. M.; Tauber, M. J.; Castro-Neto, A. H.; Lau, C. N.; Keilmann, F.; Basov, D. N. Infrared Nanoscopy of Dirac Plasmons at the Graphene−SiO_2 Interface. *Nano Lett.* **2011**, *11*, 4701−4705.
(20) Brar, V. W.; Jang, M. S.; Sherrott, M.; Lopez, J. J.; Atwater, H. Highly Confined Tunable Mid-Infrared Plasmonics in Graphene Nanoresonators. *Nano Lett.* **2013**, *13*, 2541−2547.
(21) Fang, Z.; Thongrattanasiri, S.; Schlather, A.; Liu, Z.; Ma, L.; Wang, Y.; Ajayan, P.; Nordlander, P.; Halas, N. J.; de Abajo, F. J. G. Gated Tunability and Hybridization of Localized Plasmons in Nanostructured Graphene. *ACS Nano* **2013**, *7*, 2388−2395.
(22) Gao, W.; Shi, G.; Jin, Z.; Shu, J.; Zhang, Q.; Vajtai, R.; Ajayan, P. M.; Kono, J.; Xu, Q. Excitation and Active Control of Propagating Surface Plasmon Polaritons in Graphene. *Nano Lett.* **2013**, *13*, 3698−3702.
(23) Fei, Z.; Rodin, A. S.; Andreev, G. O.; Bao, W.; McLeod, A. S.; Wagner, M.; Zhang, L. M.; Zhao, Z.; Thiemens, M.; Dominguez, G.; Fogler, M. M.; Castro Neto, A. H.; Lau, C. N.; Keilmann, F.; Basov, D. N. Gate-Tuning of Graphene Plasmons Revealed by Infrared Nano-Imaging. *Nature* **2012**, *487*, 82−85.
(24) Chen, J.; Badioli, M.; Alonso-González, P.; Thongrattanasiri, S.; Huth, F.; Osmond, J.; Spasenović, M.; Centeno, A.; Pesquera, A.; Godignon, P.; Elorza, A. Z.; Camara, N.; García de Abajo, F. J.; Hillenbrand, R.; Koppens, F. H. L. Optical Nano-Imaging of Gate-Tunable Graphene Plasmons. *Nature* **2012**, *487*, 77−81.
(25) Yan, H.; Low, T.; Zhu, W.; Wu, Y.; Freitag, M.; Li, X.; Guinea, F.; Avouris, P.; Xia, F. Damping Pathways of Mid-Infrared Plasmons in Graphene Nanostructures. *Nat. Photonics* **2013**, *7*, 394−399.
(26) Yan, H.; Li, X.; Chandra, B.; Tulevski, G.; Wu, Y.; Freitag, M.; Zhu, W.; Avouris, P.; Xia, F. Tunable Infrared Plasmonic Devices Using Graphene/Insulator Stacks. *Nat. Nanotechnol.* **2012**, *7*, 330−334.
(27) Fei, Z.; Rodin, A. S.; Gannett, W.; Dai, S.; Regan, W.; Wagner, M.; Liu, M. K.; McLeod, A. S.; Dominguez, G.; Thiemens, M.; Castro

DOI: 10.1021/acsphotonics.7b00477
ACS Photonics 2017, 4, 2971−2977

Neto, A. H.; Keilmann, F.; Zettl, A.; Hillenbrand, R.; Fogler, M. M.; Basov, D. N. Electronic and Plasmonic Phenomena at Graphene Grain Boundaries. *Nat. Nanotechnol.* **2013**, *8*, 821−825.
(28) Strait, J. H.; Nene, P.; Chan, W.-M.; Manolatou, C.; Tiwari, S.; Rana, F.; Kevek, J. W.; McEuen, P. L. Confined Plasmons in Graphene Microstructures: Experiments and Theory. *Phys. Rev. B: Condens. Matter Mater. Phys.* **2013**, *87*, 241410.
(29) Gerber, J. A.; Berweger, S.; O'Callahan, B. T.; Raschke, M. B. Phase-Resolved Surface Plasmon Interferometry of Graphene. *Phys. Rev. Lett.* **2014**, *113*, 055502.
(30) Fei, Z.; Goldflam, M. D.; Wu, J.-S.; Dai, S.; Wagner, M.; McLeod, A. S.; Liu, M. K.; Post, K. W.; Zhu, S.; Janssen, G. C. A. M.; Fogler, M. M.; Basov, D. N. Edge and Surface Plasmons in Graphene Nanoribbons. *Nano Lett.* **2015**, *15*, 8271−8276.
(31) Fei, Z.; Foley, J. J., IV; Gannett, W.; Liu, M. K.; Dai, S.; Ni, G. X.; Zettl, A.; Fogler, M. M.; Wiederrecht, G. P.; Gray, S. K.; Basov, D. N. Ultraconfined Plasmonic Hotspots Inside Graphene Nanobubbles. *Nano Lett.* **2016**, *16*, 7842−7848.
(32) Nikitin, A. Y.; Alonso-González, P.; Vélez, S.; Mastel, S.; Centeno, A.; Pesquera, A.; Zurutuza, A.; Casanova, F.; Hueso, L. E.; Koppens, F. H. L.; Hillenbrand, R. Real-Space Mapping of Tailored Sheet and Edge Plasmons in Graphene Nanoresonators. *Nat. Photonics* **2016**, *10*, 239−24.
(33) Woessner, A.; Lundeberg, M. B.; Gao, Y.; Principi, A.; Alonso-González, P.; Carrega, M.; Watanabe, K.; Taniguchi, T.; Vignale, G.; Polini, M.; Hone, J.; Hillenbrand, R.; Koppens, F. H. L. Highly Confined Low-Loss Plasmons in Graphene−Boron Nitride Heterostructures. *Nat. Mater.* **2015**, *14*, 421−425.
(34) Wang, Z.; Li, T.; Almdal, K.; Asger Mortensen, N.; Xiao, S.; Ndoni, S. Experimental Demonstration of Graphene Plasmons Working Close to the Near-Infrared Window. *Opt. Lett.* **2016**, *41*, 5345−5348.
(35) Alonso-González, P.; Nikitin, A. Y.; Gao, Y.; Woessner, A.; Lundeberg, M. B.; Principi, A.; Forcellini, N.; Yan, W.; Vélez, S.; Huber, A. J.; Watanabe, K.; Taniguchi, T.; Casanova, F.; Hueso, L. E.; Polini, M.; Hone, J.; Koppens, F. H. L.; Hillenbrand, R. Acoustic Terahertz Graphene Plasmons Revealed by Photocurrent Nanoscopy. *Nat. Nanotechnol.* **2016**, *12*, 31−35.
(36) Wagner, M.; Fei, Z.; McLeod, A. S.; Rodin, A. S.; Bao, W.; Iwinski, E. G.; Zhao, Z.; Goldflam, M.; Liu, M.; Dominguez, G.; Thiemens, M.; Fogler, M. M.; Castro Neto, A. H.; Lau, C. N.; Amarie, S.; Keilmann, F.; Basov, D. N. Ultrafast and Nanoscale Plasmonic Phenomena in Exfoliated Graphene Revealed by Infrared Pump−Probe Nanoscopy. *Nano Lett.* **2014**, *14*, 894−900.
(37) Ni, G. X.; Wang, L.; Goldflam, M. D.; Wagner, M.; Fei, Z.; McLeod, A. S.; Liu, M. K.; Keilmann, F.; Özyilmaz, B.; Castro Neto, A. H.; Hone, J.; Fogler, M. M.; Basov, D. N. Ultrafast Optical Switching of Infrared Plasmon Polaritons in High-Mobility Graphene. *Nat. Photonics* **2016**, *10*, 244−247.
(38) Crassee, I.; Orlita, M.; Potemski, M.; Walter, A. L.; Ostler, M.; Seyller, T.; Gaponenko, I.; Chen, J.; Kuzmenko, A. B. Intrinsic Terahertz Plasmons and Magnetoplasmons in Large Scale Monolayer Graphene. *Nano Lett.* **2012**, *12*, 2470−2474.
(39) Yan, H.; Li, Z.; Li, X.; Zhu, W.; Avouris, P.; Xia, F. Infrared Spectroscopy of Tunable Dirac Terahertz Magneto-Plasmons in Graphene. *Nano Lett.* **2012**, *12*, 3766−3771.
(40) Poumirol, J. M.; Yu, W.; Chen, X.; Berger, C.; de Heer, W. A.; Smith, M. L.; Ohta, T.; Pan, W.; Goerbig, M. O.; Smirnov, D.; Jiang, Z. Magnetoplasmons in Quasineutral Epitaxial Graphene Nanoribbons. *Phys. Rev. Lett.* **2013**, *110*, 246803.
(41) Dai, S.; Ma, Q.; Liu, M. K.; Andersen, T.; Fei, Z.; Goldflam, M. D.; Wagner, M.; Watanabe, K.; Taniguchi, T.; Thiemens, M.; Keilmann, F.; Janssen, G. C. A. M.; Zhu, S.; Jarillo-Herrero, P.; Fogler, M. M.; Basov, D. N. Graphene on Hexagonal Boron Nitride As a Tunable Hyperbolic Metamaterial. *Nat. Nanotechnol.* **2015**, *10*, 682−686.
(42) Brar, V. W.; Jang, M. S.; Sherrott, M.; Kim, S.; Lopez, J. J.; Kim, L. B.; Choi, M.; Atwater, H. Hybrid Surface-Phonon-Plasmon Polariton Modes in Graphene/Monolayer h-BN Heterostructures. *Nano Lett.* **2014**, *14*, 3876−3880.
(43) Yang, X.; Zhai, F.; Hu, H.; Hu, D.; Liu, R.; Zhang, S.; Sun, M.; Sun, Z.; Chen, J.; Dai, Q. Far-Field Spectroscopy and Near-Field Optical Imaging of Coupled Plasmon−Phonon Polaritons in 2D van der Waals Heterostructures. *Adv. Mater.* **2016**, *28*, 2931−2938.
(44) Li, Y.; Yan, H.; Farmer, D. B.; Meng, X.; Zhu, W.; Osgood, R. M.; Heinz, T. F.; Avouris, P. Graphene Plasmon Enhanced Vibrational Sensing of Surface Adsorbed Layers. *Nano Lett.* **2014**, *14*, 1573.
(45) Rodrigo, D.; Limaj, O.; Janner, D.; Etezadi, D.; Javier García de Abajo, F.; Pruneri, V.; Altug, H. Mid-Infrared Plasmonic Biosensing with Graphene. *Science* **2015**, *349*, 165−168.
(46) Hu, H.; Yang, X.; Zhai, F.; Hu, D.; Liu, R.; Liu, K.; Sun, Z.; Dai, Q. Far-Field Nanoscale Infrared Spectroscopy of Vibrational Fingerprints of Molecules with Graphene Plasmons. *Nat. Commun.* **2016**, *7*, 12334.
(47) Vakil, A.; Engheta, N. Transformation Optics Using Graphene. *Science* **2011**, *332*, 1291−1294.
(48) Lu, W. B.; Zhu, W.; Xu, H. J.; Ni, Z. H.; Dong, Z. G.; Cui, T. J. Flexible Transformation Plasmonics Using Graphene. *Opt. Express* **2013**, *21*, 10475−10482.
(49) Zeng, C.; Liu, X.; Wang, G. Electrically Tunable Graphene Plasmonic Quasicrystal Metasurfaces for Transformation Optics. *Sci. Rep.* **2014**, *4*, 5763.
(50) Huidobro, P. A.; Kraft, M.; Kun, R.; Maier, S. A.; Pendry, J. B. Graphene, Plasmons and Transformation Optics. *J. Opt.* **2016**, *18*, 044024.
(51) McLeod, A. S.; Kelly, P.; Goldflam, M. D.; Gainsforth, Z.; Westphal, A. J.; Dominguez, G.; Thiemens, M. H.; Fogler, M. M.; Basov, D. N. Model for Quantitative Tip-Enhanced Spectroscopy and the Extraction of Nanoscale-Resolved Optical Constants. *Phys. Rev. B: Condens. Matter Mater. Phys.* **2014**, *90*, 085136.
(52) Knoll, B.; Keilmann, F. Enhanced Dielectric Contrast in Scattering-Type Scanning Near-Field Optical Microscopy. *Opt. Commun.* **2000**, *182*, 321−328.
(53) Hillenbrand, R.; Keilmann, F. Complex Optical Constants on a Subwavelength Scale. *Phys. Rev. Lett.* **2000**, *85*, 3029−3032.
(54) Ocelic, N.; Huber, A.; Hillenbrand, R. Pseudoheterodyne Detection for Background-Free Near-Field Spectroscopy. *Appl. Phys. Lett.* **2006**, *89*, 101124.
(55) Jiang, B.-Y.; Ni, G. X.; Pan, C.; Fei, Z.; Cheng, B.; Lau, C. N.; Bockrath, M.; Basov, D. N.; Fogler, M. M. Tunable Plasmonic Reflection by Bound 1D Electron States in a 2D Dirac Metal. *Phys. Rev. Lett.* **2016**, *117*, 086801.
(56) Huang, P. Y.; Ruiz-Vargas, C. S.; van der Zande, A. M.; Whitney, W. S.; Levendorf, M. P.; Kevek, J. W.; Garg, S.; Alden, J. S.; Hustedt, C. J.; Zhu, Y.; Park, J.; McEuen, P. L.; Muller, D. A. Grains and Grain Boundaries in Single-Layer Graphene Atomic Patchwork Quilts. *Nature* **2011**, *469*, 389−392.
(57) Li, X.; Cai, W.; An, J.; Kim, S.; Nah, J.; Yang, D.; Piner, R.; Velamakanni, A.; Jung, I.; Tutuc, E.; Banerjee, S. K.; Colombo, L.; Ruoff, R. S. Large-Area Synthesis of High-Quality and Uniform Graphene Films on Copper Foils. *Science* **2009**, *324*, 1312−1314.
(58) Alonso-González, P.; Nikitin, A. Y.; Golmar, F.; Centeno, A.; Pesquera, A.; Vélez, S.; Chen, J.; Navickaite, G.; Koppens, F.; Zurutuza, A.; Casanova, F.; Hueso, L. E.; Hillenbrand, R. Controlling Graphene Plasmons with Resonant Metal Antennas and Spatial Conductivity Patterns. *Science* **2014**, *344*, 1369−1373.
(59) Fei, Z.; Iwinski, E. G.; Ni, G. X.; Zhang, L. M.; Bao, W.; Rodin, A. S.; Lee, Y.; Wagner, M.; Liu, M. K.; Dai, S.; Goldflam, M. D.; Thiemens, M.; Keilmann, F.; Lau, C. N.; Castro-Neto, A. H.; Fogler, M. M.; Basov, D. N. Tunneling Plasmonics in Bilayer Graphene. *Nano Lett.* **2015**, *15*, 4973−4978.
(60) Ni, G. X.; Wang, H.; Wu, J. S.; Fei, Z.; Goldflam, M. D.; Keilmann, F.; Özyilmaz, B.; Castro Neto, A. H.; Xie, X. M.; Fogler, M. M.; Basov, D. N. Plasmons in Graphene Moiré Superlattices. *Nat. Mater.* **2015**, *14*, 1217−1222.
(61) Xue, J.; Sanchez-Yamagishi, J.; Bulmash, D.; Jacquod, P.; Deshpande, A.; Watanabe, K.; Taniguchi, T.; Jarillo-Herrero, P.;

DOI: 10.1021/acsphotonics.7b00477
ACS Photonics 2017, 4, 2971−2977

LeRoy, B. J. Scanning Tunnelling Microscopy and Spectroscopy of Ultra-Flat Graphene on Hexagonal Boron Nitride. *Nat. Mater.* **2011**, *10*, 282−285.
(62) Dean, C. R.; Wang, L.; Maher, P.; Forsythe, C.; Ghahari, F.; Gao, Y.; Katoch, J.; Ishigami, M.; Moon, P.; Koshino, M.; Taniguchi, T.; Watanabe, K.; Shepard, K. L.; Hone, J.; Kim, P. Hofstadter's Butterfly and the Fractal Quantum Hall Effect in Moiré Superlattices. *Nature* **2013**, *497*, 598−602.
(63) Wallbank, J. R.; Patel, A. A.; Mucha-Kruczyński, M.; Geim, A. K.; Fal'ko, V. I. Generic Miniband Structure of Graphene on a Hexagonal Substrate. *Phys. Rev. B: Condens. Matter Mater. Phys.* **2013**, *87*, 245408.
(64) Shi, Z.; Jin, C.; Yang, W.; Ju, L.; Horng, J.; Lu, X.; Bechtel, H. A.; Martin, M. C.; Fu, D.; Wu, J.; Watanabe, K.; Taniguchi, T.; Zhang, Y.; Bai, X.; Wang, E.; Zhang, G.; Wang, F. Gate-Dependent Pseudospin Mixing in Graphene/Boron Nitride Moiré Superlattices. *Nat. Phys.* **2014**, *10*, 743−747.
(65) Gorbachev, R. V.; Song, J. C. W.; Yu, G. L.; Kretinin, A. V.; Withers, F.; Cao, Y.; Mishchenko, A.; Grigorieva, I. V.; Novoselov, K. S.; Levitov, L. S.; Geim, A. K. Detecting Topological Currents in Graphene Superlattices. *Science* **2014**, *346*, 448−451.
(66) Chen, Z.-G.; Shi, Z.; Yang, W.; Lu, X.; Lai, Y.; Yan, H.; Wang, F.; Zhang, G.; Li, Z. Observation of an Intrinsic Bandgap and Landau Level Renormalization in Graphene/Boron-Nitride Heterostructures. *Nat. Commun.* **2014**, *5*, 4461.
(67) Schnell, M.; Carney, P. S.; Hillenbrand, R. Synthetic Optical Holography for Rapid Nanoimaging. *Nat. Commun.* **2014**, *5*, 3499.
(68) Zhang, L. M.; Andreev, G. O.; Fei, Z.; McLeod, A. S.; Dominguez, G.; Thiemens, M.; Castro-Neto, A. H.; Basov, D. N.; Fogler, M. M. Near-Field Spectroscopy of Silicon Dioxide Thin Films. *Phys. Rev. B: Condens. Matter Mater. Phys.* **2012**, *85*, 075419.
(69) Jiang, B.-Y.; Zhang, L. M.; Castro Neto, A. H.; Basov, D. N.; Fogler, M. M. Generalized spectral method for near-field optical microscopy. *J. Appl. Phys.* **2016**, *119*, 054305.
(70) Shi, Z.; Hong, X.; Bechtel, H. A.; Zeng, B.; Martin, M. C.; Watanabe, K.; Taniguchi, T.; Shen, Y.-R.; Wang, F. Observation of a Luttinger-Liquid Plasmon in Metallic Single-Walled Carbon Nanotubes. *Nat. Photonics* **2015**, *9*, 515.
(71) Chen, J.-H.; Autes, G.; Alem, N.; Gargiulo, F.; Gautam, A.; Linck, M.; Kisielowski, C.; Yazyev, O. V.; Louie, S. G.; Zettl, A. Controlled Growth of a Line Defect in Graphene and Implications for Gate-Tunable Valley Filtering. *Phys. Rev. B: Condens. Matter Mater. Phys.* **2014**, *89*, 121407.
(72) Alexandre, S. S.; Lúcio, A. D.; Castro Neto, A. H.; Nunes, R. W. Correlated Magnetic States in Extended One-Dimensional Defects in Graphene. *Nano Lett.* **2012**, *12*, 5097−5102.
(73) Yazyev, O. V.; Louie, S. G. Topological Defects in Graphene: Dislocations and Grain Boundaries. *Phys. Rev. B: Condens. Matter Mater. Phys.* **2010**, *81*, 195420.
(74) Barja, S.; Wickenburg, S.; Liu, Z.-F.; Zhang, Y.; Ryu, H.; Ugeda, M. M.; Hussain, Z.; Shen, Z.-X.; Mo, S.-K.; Wong, E.; Salmeron, M. B.; Wang, F.; Crommie, M. F.; Ogletree, D. F.; Neaton, J. B.; Weber-Bargioni, A. Charge Density Wave Order in 1D Mirror Twin Boundaries of Single-Layer $MoSe_2$. *Nat. Phys.* **2016**, *12*, 751−756.
(75) Woessner, A.; Alonso-González, P.; Lundeberg, M. B.; Gao, Y.; Barrios-Vargas, J. E.; Navickaite, G.; Ma, Q.; Janner, D.; Watanabe, K.; Cummings, A. W.; Taniguchi, T.; Pruneri, V.; Roche, S.; Jarillo-Herrero, P.; Hone, J.; Hillenbrand, R.; Koppens, F. H. L. Near-Field Photocurrent Nanoscopy on Bare and Encapsulated Graphene. *Nat. Commun.* **2016**, *7*, 10783.
(76) Ju, L.; Shi, Z.; Nair, N.; Lv, Y.; Jin, C.; Velasco, J., Jr; Ojeda-Aristizabal, C.; Bechtel, H. A.; Martin, M. C.; Zettl, A.; Analytis, J.; Wang, F. Topological Valley Transport at Bilayer Graphene Domain Walls. *Nature* **2015**, *520*, 650−655.
(77) Jiang, L.; Shi, Z.; Zeng, B.; Wang, S.; Kang, J.-H.; Joshi, T.; Jin, C.; Ju, L.; Kim, J.; Lyu, T.; Shen, Y.-R.; Crommie, M.; Gao, H.-J.; Wang, F. Soliton-Dependent Plasmon Reflection at Bilayer Graphene Domain Walls. *Nat. Mater.* **2016**, *15*, 840−844.
(78) Williams, J. R.; DiCarlo, L.; Marcus, C. M. Quantum Hall Effect in a Gate-Controlled p-n Junction of Graphene. *Science* **2007**, *317*, 638−641.
(79) Cheianov, V. V.; Fal'ko, V.; Altshuler, B. L. The Focusing of Electron Flow and a Veselago Lens in Graphene p-n Junctions. *Science* **2007**, *315*, 1252−1255.
(80) Stander, N.; Huard, B.; Goldhaber-Gordon, D. Evidence for Klein Tunneling in Graphene p−n Junctions. *Phys. Rev. Lett.* **2009**, *102*, 026807.
(81) Nemilentsau, A.; Low, T.; Hanson, G. Anisotropic 2D materials for Tunable Hyperbolic Plasmonics. *Phys. Rev. Lett.* **2016**, *116*, 066804.

DOI: 10.1021/acsphotonics.7b00477
ACS Photonics 2017, 4, 2971−2977